Reviewer #3 (Vasileios Chatzaras)

Major comments

1) What are the implications of the described melt-rock interactions on the mechanical behaviour of STEP faults? The sampled suite of xenoliths offers unique insights into processes that take place in the mantle section of a STEP fault, so the Authors could go one step further and explore how the described microtectonic evolution may have affected mantle strength and rheology. For example, the Authors could use the olivine subgrain size, which is mentioned in the Methods section but not included in the manuscript, to determine the stress levels at different depths of the lithosphere. In samples where the microstructures are controlled by dynamic recrystallization, the olivine recrystallized grain size could be used, as well.

The analysis of the olivine subgrain size provided ambiguous results, therefore, we decided not to include it in the manuscript and the database. The reference to this data in the methodology chapter is a mistake but we removed it from the revised text. As for the piezometry based on the recrystallized grain size, we refer to our answer to Reviewer #2.

2) A long-standing problem in mantle xenolith studies is the lack of a clear foliation and lineation, which leads to the production of thin sections in random orientations relative to the rock shape fabric. As a result, the EBSD-derived crystallographic orientations are rotated so as to match one of the common crystallographic texture types described in the literature. Similar workflow is followed in this study. The main problem here becomes the discrimination between the different orthorhombic CPO patterns. The axial-[100], axial-[010], and orthorhombic symmetries can still be identified (e.g., with the use of the BA-index as done here) without the need to plot the crystallographic texture data relative to the rock shape fabric. As a solution to this problem, the use of X-ray Computed Tomography (XRCT) was recently proposed, where rock fabric can be determined quantitatively by the 3D shape of spinel grains (Chatzaras et al., 2016, already cited in the manuscript). In fact, to the best of my knowledge, the first paper in which XRCT was used for visual determination of the rock fabric in mantle xenoliths, was of this manuscript's first Author (Hidas et al., 2007). The Authors could use the rock billets from which the thin sections were produced to determine quantitatively the rock fabric using XRCT, and replot the EBSD data relative to the fabric reference framework. That said, here the Authors do not attempt any discrimination between the different orthorhombic CPO patterns, so their workflow is totally appropriate for the level of interpretation. It is just that the use of XRCT would provide information currently inaccessible for the analyzed xenolith suite.

We agree with the reviewer that micro-CT may provide crucial information for microstructural studies. Unfortunately, at the time when the thin sections on the Oran mantle xenoliths were made, we did not have access to micro-CT and the remaining rock chips are now too small for such analyses. Consequently, we can only use the traditional methods from the literature to differentiate between CPO patterns.

3) Olivine CPO in the coarse-grained xenoliths has a dominant axial-[100] symmetry, while it transitions toward an axial-[010] symmetry in the fine-grained xenoliths, where shearing combined with extensive synkinematic melt-rock interaction is interpreted to take place along a ductile shear zone associated with the Rif-Tell STEP fault. Based on these observations / interpretations, I am thinking of the following CPO and tectonic evolution, which the Authors may want to consider. Olivine axial-[100] CPO symmetry could be the result of constrictional strain associated with mantle upwelling in the slab window beneath the North African margin. An axial-[100] CPO pattern in both olivine and plagioclase was observed in xenoliths from the San Quintin volcanic field in Baja California (van der Werf et al., 2017), which is also interpreted to lie above a slab window (e.g., Zhang et al., 2012), similar to the Oran volcanic field. In the Oran xenoliths, mantle rocks were then captured from the inferred shear zone at the mantle section of the STEP fault. Focused melt migration along the shear zone and potential transpressional deformation (based on Figure 10) may have caused a transition of olivine CPO toward axial-[010] symmetry. The observed variations in microstructures and olivine CPOs could reflect either vertical or lateral heterogeneities in the North African SCLM.

We see no contradiction between our conceptual model on the development of olivine CPO in a melt-lubricated STEP mantle shear zone and the proposition outlined by the Reviewer. We agree with his points and we added more details on the conceptual model to the discussion (chapters 6.1.2 and 6.3) following the Reviewer's suggestions.

Chapter 6.1.2:

"…Thus, we favor the latter hypothesis that is shear deformation of olivine in the presence of melt to explain the shift towards [010]-fiber olivine patterns in the equigranular peridotites. Alternatively, the transition of olivine CPO symmetry toward axial-[010] in the fine-grained xenoliths may have developed enhanced by several of the above factors, of which the most likely scenario would be focused melt migration in a transpressional mantle shear zone, considering the geodynamic environment of the Oran volcanic field. Nevertheless, in the observed textures, the crystallographic axes of small orthopyroxenes are weakly oriented and, occasionally, distributed subparallel to those of olivine (Fig. 5b; Fig. S1)."

Chapter 6.3:

"…This deformation may either be an older event preserved in the rocks, or correspond to the lateral mantle flow from the Canary plume and mantle upwelling beneath the N-African margin, resulting in axial-[100] olivine CPO symmetry that developed due to constrictional strain. […] These results suggest that wehrlitization of the Oran SCLM is a relatively young event, which took place in late Miocene to early Pleistocene times, and the observed variations in microstructures and olivine CPOs could reflect vertical and/or lateral heterogeneities along the N-African margin…"

Minor comments

Page 1, lines 28-29: The Authors mention that grain size is "uncorrelated with modal variations", while in lines 31-32 (same page), it is mentioned that "Olivine grain size in the fine-grained peridotites depends on the size and volume fraction of the pyroxene grains". How do these statements fit together?

The grain size is uncorrelated with modal variations in the sense that it does not correlate to lithological classification, i.e., there are coarse-grained and fine-grained harzburgite or wehrlite among the studied xenoliths. Rather than lithology, the dependence of the olivine grain size on the modal content of pyroxene is clear if not only the volume fraction but the size of these second phase particles is considered as well (cf. Fig. 8). We clarified the apparent contradiction in the revised manuscript:

"…The microstructures of mantle xenoliths show a variable grain size ranging from coarse granular to fine-grained equigranular textures uncorrelated with lithology…"

Page 5, lines 11-13: Please state the exact number of samples (and identify their names) in which the thin sections were produced relative to the common structural framework (normal to foliation and parallel to lineation). Also, a suggestion for Figure S1, would be to use the horizontal line and the star (as in Figure 5) to show the foliation and lineation in the samples cut relative to the rock shape fabric.

We now indicate the oriented thin sections with an asterisk in the first column of Table 1 in the revised manuscript and we updated the supplementary Fig. S1 with the information requested by the Reviewer.

Sample	Lithology (Fabric)*	Estimated Temperature [°C][b]						Modal Composition [%]						Area-wtd Mean Grain Size [mm]			Calculated Parameters[c]			
		core			rim															
		$T_{Ca\text{-}Opx}$	$T_{Al\text{-}Opx}$	$T_{solv.}$	$T_{Ca\text{-}Opx}$	$T_{Al\text{-}Opx}$	$T_{solv.}$	Ol	Opx	Cpx	Spl	Amp	Plag	Ol	Opx	Cpx	BA	M_{Ol}	M_{Opx}	M_{Cpx}
DZ-002	HZB(CG)	950	1021	1034	1028	1002	1093	77.0	17.7	4.8	0.6			1.4	1.3	0.5	0.47	0.32	0.27	0.05
DZ-003*	LHZ(CG)	1087	955	1086	1108	991	1060	84.4	7.9	7.3	0.5			1.5	1.5	0.5	0.52	0.33	0.31	0.12
DZ-004	HZB(CG)							87.3	11.1	1.3	0.2			1.5	1.5	0.4	0.77	0.21	0.24	0.22
DZ-005*	LHZ(CGP)							86.1	6.6	6.7	0.7			1.0	1.3	0.5	0.74	0.27	0.36	0.06
DZ-007	HZB(CGP)	1023	987	999	967	889	989	86.6	8.5	4.4	0.6			1.2	1.0	0.4	0.74	0.24	0.25	0.03
DZ-009*	LHZ(CGP)	957	1063	873	911	924	851	69.5	20.0	9.9	0.6			1.2	1.8	1.2	0.79	0.19	0.15	0.14
DZ-010b	LHZ(CGP)							77.1	13.8	7.8	1.0	0.4		0.8	1.1	0.7	0.88	0.20	0.21	0.05
GU-001	LHZ(CGP)	1047	1163	907	901	890	879	75.1	9.5	14.0	1.2	0.3		1.1	2.4	0.8	0.68	0.26	0.32	0.08
GU-002	LHZ(EQ)							89.7	4.0	6.2	0.0	0.1	0.1	0.6	0.3	0.3	0.41	0.17	0.04	0.03
GU-003	HZB(CGP)							82.8	13.7	3.4	0.0			0.8	1.8	0.4	0.68	0.27	0.29	0.09
GU-007*	HZB(CGP)							87.4	9.1	3.1	0.3			1.0	1.1	0.5	0.64	0.18	0.17	0.20
HAM-001	WHR(CG)	1043	986	997	1068	1048	1057	71.4	4.3	23.9	0.4			1.3	0.7	1.0	0.77	0.17	0.16	0.07
HAM-004	HZB(EQ)							78.3	17.8	2.6	1.2	0.1	0.1	0.4	0.2	0.2	0.72	0.19	0.06	0.02
HAM-005b*	LHZ(FGP)	949	971	983	939	942	1017	80.1	12.5	6.6	0.6	0.0	0.2	0.8	0.8	0.4	0.65	0.12	0.03	0.03
HAM-006*	HZB(EQ)							81.7	15.3	2.8	0.2			0.5	0.3	0.2	0.37	0.12	0.03	0.05
HAM-007	HZB(EQ)							74.0	21.8	3.4	0.8		0.1	0.4	0.5	0.3	0.24	0.13	0.01	0.03
HAM-009	LHZ(FGP)							69.8	19.0	9.4	1.0		0.8	0.6	1.6	0.4	0.72	0.09	0.08	0.02
HAM-011	HZB(EQ)							80.8	13.0	4.7	0.5	0.6	0.4	0.4	0.3	0.2	0.35	0.18	0.01	0.02
HAM-012*	LHZ(EQ)	939	939	790	979	909	884	83.5	10.1	5.5	0.6	0.2	0.1	0.5	0.4	0.3	0.45	0.12	0.03	0.02
HAM-016	HZB(EQ)							81.9	13.6	1.4	3.0	0.1		0.6	0.3	0.2	0.67	0.20	0.05	0.04
HAM-017*	LHZ(EQ)	945	953	928	992	872	974	79.0	14.1	6.3	0.6			0.6	0.5	0.3	0.42	0.10	0.02	0.02
HAM-018	LHZ(EQ)	985	1010	842	974	931	909	54.1	12.2	32.4	0.0	0.2	0.2	0.3	0.4	0.4	0.37	0.03	0.01	0.01
SOU-001	LHZ(CGP)							75.0	16.0	8.2	0.8			1.0	1.0	0.4	0.55	0.37	0.29	0.06
SOU-002	LHZ(CG)	950	953	977	965	919	956	53.2	26.3	17.5	2.9	0.1		0.9	2.0	1.0	0.64	0.22	0.14	0.04
SOU-003	WHR(CG)	-	-		-	-		89.5	0.0	9.7	0.8			1.3	0.2	0.7	0.39	0.21		0.06

[a]Lithology: HZB, harzburgite; LHZ, lherzolite; WHR, wehrlite/(Fabric): CG, coarse granular; CGP, coarse-grained porphyrodastic; FGP, fine-grained porphyroclastic; EQ, fine-grained equigranular. [b]$T_{Ca\text{-}Opx}$: Ca-in-orthopyroxene (±16°C), Brey and Köhler (1990); $T_{Al\text{-}Opx}$: Cr-Al-orthopyroxene (±15°C), Witt-Eickschen and Seck (1991); $T_{solv.}$ clinopyroxene-orthopyroxene geothermometer (±16°C), Brey and Köhler (1990). [c]BA, BA-index of olivine; M_{Ol}, M-index of olivine; M_{Opx}, M-index of orthopyroxene; M_{Cpx}, M-index of clinopyroxene (Skemer et al., 2005). *Oriented thin section.

Page 6, Lines 5-7: I don't think that the Authors present in the manuscript the calculations of the subgrain boundaries length and subgrain density mentioned here. Either remove this description or include the results in the manuscript. Having said that, I think that the manuscript would benefit from the inclusion of these data if subgrain size is used for estimating differential stress. See comment 1.

During the compilation of the manuscript, we attempted to calculate the subgrain size and subgrain densities from EBSD data but the results are highly influenced by analytical artifacts (e.g., charging in some critical xenoliths) and are also moderately dependent on the step size of the EBSD maps. Consequently, we decided not to use this ambiguous data in the final version

but the corresponding description has been accidentally left in the methods chapter. We removed this part from the revised version.

As for the estimation of differential stress based on recrystallized grain size, we refer to our answer to the related comment of Reviewer #2.

Page 6, Lines 8-17: Following on the previous comment, the KAM2, Mis2Mean, and GOS data described here are not presented in the manuscript. Exception is Figure 3, where two Mis2Mean maps are included. The Authors may want to revise the Methods section removing the description of these parameters. Alternatively, they could use the data to describe the microstructural characteristics of different mineral phases and grain sizes.

Discussing all the calculated parameters is beyond the scope of the research and, in the manuscript, we address only the most important ones. We nevertheless include the results of the calculations in a database, which is provided as supplementary material. In the revised version, we refer to the corresponding table:*"… For the complete database of calculated parameters, see Table S1. .."*

Page 8, Line 19: Please mention some sample names in which the reader can observe the feature you describe here (elongated patches of clinopyroxene aggregates). It would also be useful to highlight these features in the relevant EBSD phase maps.

We refer to some characteristic samples in the revised manuscript: *"…Clinopyroxene may also form large crystals that are not porphyroclasts but aggregates of several millimetric crystals in elongated patches in the plane of the foliation (e.g., xenoliths GU-001, HAM-001, HAM-009; Fig. S1)…"*

Page 8, Line 21: "Strain-free" is an interpretation. Please describe the observations that lead to this interpretation.

We added the observations that led to the interpretation: *"...Large pyroxenes are rarely observed in the equigranular texture. On the other hand, both pyroxenes occur as a fine-grained, elongated (with breadth <100 microns) mineral fraction free from petrographic signs of intracrystalline lattice distortion and usually dispersed in the rocks without showing textural preference to porphyroclasts…"*

Page 8, Line 23: Please highlight on the photomicrograph or EBSD map of Figure 3 these cusp-like terminations at triple junctions.

We indicate representative examples of irregularly shaped small pyroxenes that are distributed at olivine-olivine grain boundaries, or have cusp-like termination at triple junctions in the revised Fig. 3e:

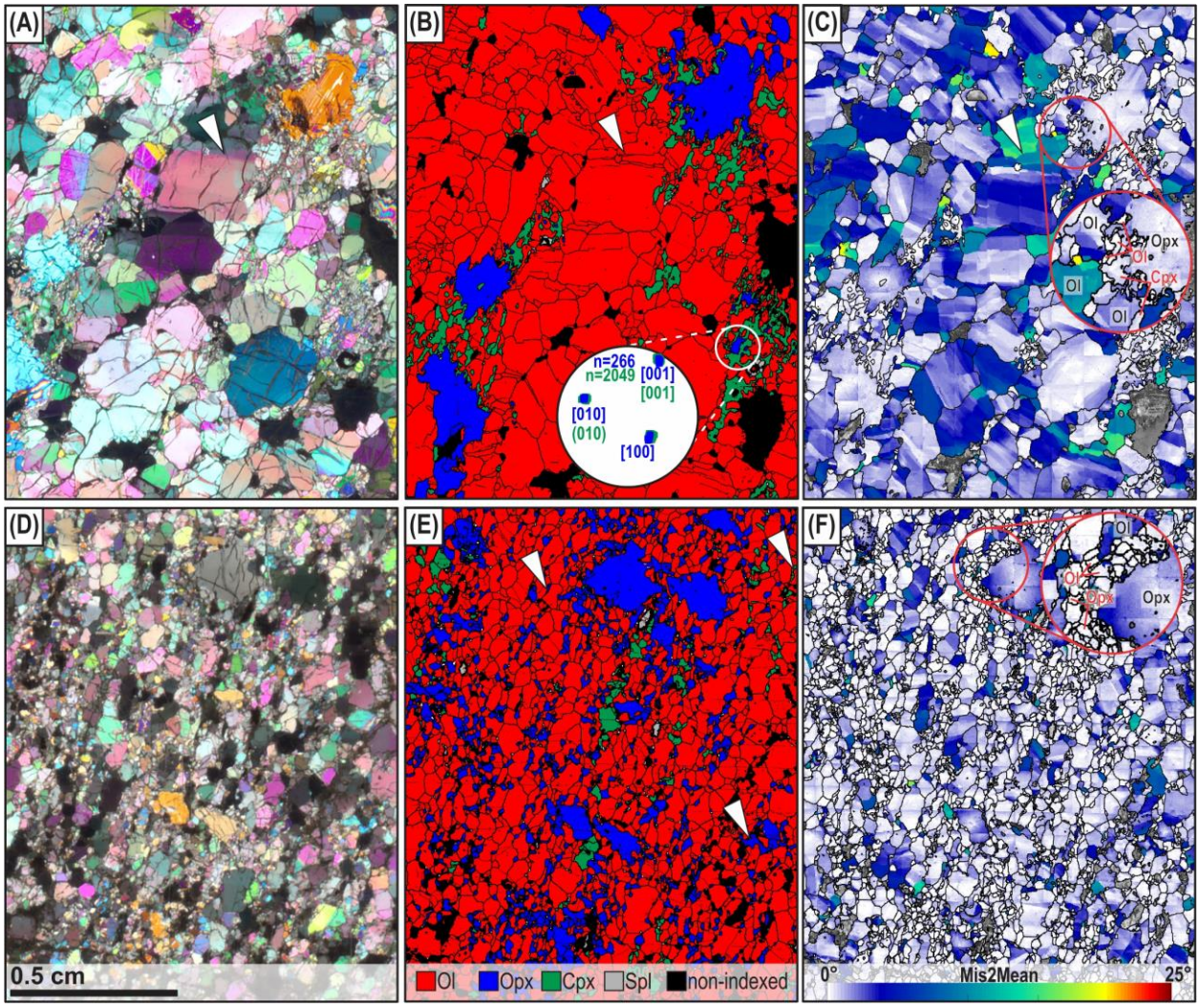

Page 8, Line 27: "locally showing reaction microstructure" is an interpretation. What are the relevant microscale observations?

We clarified the description in the revised manuscript: *"…In some clinopyroxene-rich depleted lherzolite (e.g., DZ-003), the fine-grained clinopyroxene occur as a rim on orthopyroxene porphyroclasts with irregular phase boundaries and identical crystallographic orientation of the two pyroxenes (Fig. 3b)…"*

Page 9, Lines 16-18: Please be more specific to which samples in Figure 5b you refer. HAM-005b does not show an axial-[010] symmetry.

We refer to a representative sample in the revised manuscript: *"…In the orthorhombic CPO symmetries that show tendency towards [010]-fiber pattern, typical for some fine-grained xenoliths, we observe a strong maximum of [010] perpendicular to the foliation and a very weak girdle of [100] and [001] axes in the plane of the foliation (e.g., sample HAM-007 in Fig. 5b)…"*

Page 9, Lines 26-27: Looking the CPO plots, and particularly those of DZ-003, which is the oriented thin section, I am not convinced that this is the case. The maximum of the orthopyroxene [100] axes lies within the foliation plane at high angle to the lineation, although two smaller concentrations near the pole to the foliation are also present. Moreover, please mention which are the oriented thin sections so that the reader can track the information mentioned in the text.

We agree with the reviewer that there are two point-like maxima of [100]-axes in xenolith DZ-003. The apparently stronger maximum at a high angle to the lineation in the plane of the foliation, however, belongs to a few (<5) coarse orthopyroxene crystals and their remnants that have been left behind in their surroundings after the original porphyroclast was reacted to form secondary clinopyroxene ±olivine (Fig. R1). This fragmentation results in anomalously high-density contours in the pole figures related to these few, similarly oriented crystal aggregates that otherwise represent only a minority of the orthopyroxene population. This issue is typical for coarse-grained microstructures where the number of grains of a given mineral phase is limited, and even a minor over-segmentation can result in anomalously high contour densities. In our case, the increased number of similarly oriented orthopyroxene crystals is due to the melt-rock reaction that left behind some small orthopyroxene crystals from the original porphyroclast (e.g., inset in Fig. R1). We nevertheless did not want to delete any data points or artificially modify the dataset but we kept this artifact in mind when presenting the CPO data of this sample in the text. The second maximum in Fig. 5 of the manuscript, which has the [100]-axes distributed at the pole of the foliation, comes from various grains and supports our description provided in page 9, lines 26-27 of the original manuscript.

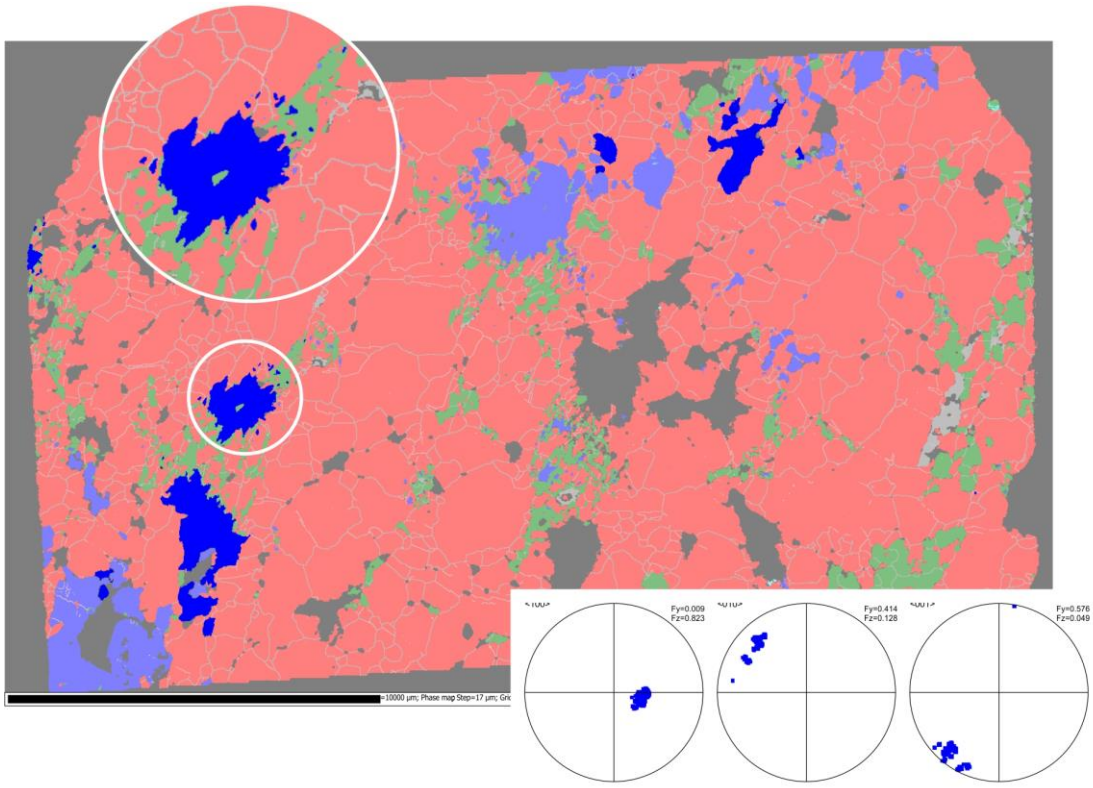

Fig. R1: *Phase map of xenolith DZ-003 highlighting only those orthopyroxene crystals (in vivid blue) that have anomalous orientations Fig. 5 of the manuscript. In the pole figure only the orientation of these crystals are shown. Inset highlights a coarse orthopyroxene crystal with its remnants left behind after orthopyroxene-consuming melt-rock reaction. For the full dataset, see Fig. 5 and Fig. S1 of the manuscript.*

Page 9, Lines 29-30: If orthopyroxene [010] and [001] axes are distributed subparallel to olivine [010] and [001] axes, we would expect the same relationship to hold for the [100] axes, as well. This is not the case in HAM-007, where olivine [100] axes are oriented at high angle to orthopyroxene [100] axes.

The subparallel distribution between olivine and orthopyroxene crystallographic axes is the strongest in the [010] axes, while the other two main crystallographic axes are more dispersed. We do not know the exact mechanism that results in such a crystallographic relationship between olivine and orthopyroxene but the observation is not new in the literature. We agree with the reviewer and we clarified the description in the revised manuscript: *"…In the fine-grained rocks —particularly in the equigranular samples— the main crystallographic axes of orthopyroxene are generally distributed subparallel to those of olivine (e.g., $[010]_{Ol}$ || $[010]_{Opx}$ in xenoliths HAM-007 and HAM-018 in Fig. 5b). Such subparallel distribution is characteristic mostly for [010]- and, less frequently, [100]- or [001]-axes…"*

Page 10, Lines 4-5: In methods, the Authors describe a 2-12° range for subgrain boundaries, so I am wondering why they chose a different range of angles to analyse low-angle misorientations. Moreover, could the Authors explain the criteria for choosing the 400 μm grain size threshold for the misorientation analysis? Earlier on (page 8, lines 2-3), they defined the coarse and fine grained porphyroclasts based on a 800 μm grain size threshold.

The difference in the range for defining subgrain boundaries is an error, the correct one is indeed 2-12° and we applied these values during data analysis. We corrected the range in the revised version.

Both threshold values are empirical and serve to identify features of interest in a given analysis. For the textural classification, the ca. 800 μm threshold (expressed as area-weighted average grain size; Fig. 2) in olivine worked the best to differentiate the fine-grained and coarse-grained xenolith textures from each other (page 8, lines 2-3). Note that the area-weighted average grain size is a single value per mineral phase in a given xenolith. However, in the analysis of rotation axes accommodating low-angle misorientations, the emphasis was put rather on the pyroxenes than on olivine, considering that in olivine the rotation axes show <0vw> orientations irrespective of the grain size (page 10, lines 6-8 of the original manuscript). For this purposes, the 400 μm threshold (expressed as equivalent diameter) allowed us to correctly differentiate the two distinct populations of pyroxenes presented in the petrography, and to carry out their detailed analyses. Note that in the petrographic description of the fine-grained pyroxenes the <100 microns diameter (page 8, line 20 of the original manuscript) refers to the breadth of crystals, whereas in the analysis of rotation axes the threshold corresponds to their equivalent diameter. As stated before, in case of olivine our choice of empirical value has no impact on the results and we made the nature of the threshold values clear in the revised manuscript: *"…Based on the average grain size of olivine in these transitional textures, we distinguish coarse-grained porphyroclastic (olivine >0.8 mm area-weighted average grain size; 8 samples, 32%) and fine-grained porphyroclastic texture types (olivine <0.8 mm area-weighted average grain size; 2 samples, 8%) (Fig. 2b). […] On the other hand, both pyroxenes occur as a fine-grained, elongated (with breadth <100 microns) mineral fraction free from petrographic signs of intracrystalline lattice distortion and usually dispersed in the rocks without showing textural preference to porphyroclasts…"*

Page 11, Lines 16-17: I agree with this statement only for the coarse-grained xenoliths (green color). When it comes to the rest three microstructural types, I do not see a clear trend. I am wondering whether a plot of grain size versus estimated temperature would help the Authors to make their argument more clear. This is quite important point, because if there is no clear positive correlation between grain size and temperature, the Authors might want to consider the possibility that the xenoliths sample a horizontal strain gradient across the STEP fault. I am also wondering whether any fine-grained xenoliths have been reported from Souahlia. The lack of fine-grained xenoliths might be indicative of an horizontal strain gradient between Souahlia and Ain Temouchent.

As Fig. 2b reflects, there is a homogenization of grain size from the coarse-grained to the fine-grained textures. The textural classification of the xenoliths is based on this figure, thus the grouping of samples by texture in Fig. 7b already contains correlation of the calculated temperatures with olivine grain size. Nevertheless, Fig. 2b also reflects that, particularly in the

porphyroclastic samples, significant differences may exist between the grain size of olivine and pyroxenes. Therefore, we do not know to which grain size the temperature should be compared in a diagram proposed by the reviewer (maximum/average porphyroclast, median, or average small grains, to name a few possibilities). We are also wondering on the expected trend on this diagram that could unambiguously support/eliminate the existence of horizontal strain gradients in the Oran SCLM. We believe that such a plot would not provide information on this question and, consequently, we have not changed the corresponding figure.

Finally, we have not found fine-grained xenoliths in Souahlia but mantle xenoliths are less frequent in this outcrop than elsewhere in Oran, therefore we prefer not to conclude that this texture type is not present in the mantle beneath the locality.

Page 11, Lines 25-27: Some more information regarding the calculation of the Zener parameter might be useful to be included in the manuscript. Specifically, were all orthopyroxene and clinopyroxene grains in each sample included in the analysis, or porphyroclasts were excluded? In the latter case, what was the maximum size of grains included? Moreover, I am not sure that we can separate the contribution of orthopyroxene and clinopyroxene grains to the pining of olivine grains. In the current analysis, the underlying assumption is that the only second phase is either orthopyroxene or clinopyroxene, and the rest area/volume is occupied mainly by olivine. Such assumption could work for samples with only a small fraction of the other pyroxene. Otherwise, the two pyroxenes should be considered together.

In fact, the idea with the analysis presented in Fig. 8 is to see if the olivine grain size was controlled by the presence of second phase particles due to pinning. For the sake of simplicity, we consider only pyroxenes in this analysis, as the total amount of spinel, plagioclase and amphibole does not exceed a few modal percents in the studied xenoliths and their mixing with olivine is negligible compared to the pyroxenes. In the analysis, we intentionally decided to address the role of pyroxenes separately and no grains have been left out from the calculations. The main message of these diagrams is that (1) pyroxenes exerted pinning on the olivine grain size particularly in the fine-grained xenoliths, and (2) the two pyroxenes might have a different effect in the coarse-grained textures. Evidently, if both pyroxenes were presented together in a single diagram, the overall distribution would not change but it would be impossible to recognize this subtle difference between the behavior of clinopyroxene and orthopyroxene in the coarse-grained xenoliths. We believe that the current version of the analyses provides more insights into the pinning effect and, consequently, we decided not to merge the clinopyroxenes and orthopyroxenes in a single pyroxene database.

Page 12, Lines 3-4: In agreement with Figure 8, the Authors state here that olivine grain growth is impeded by the small, interstitial pyroxene grains. However, in page 8, lines 25-26, it is mentioned that in the xenoliths with an equigranular microstructure, the small pyroxene grains "occur in monophase patches rather than showing phase mixing", which is actually not what we see in the cited Figure 3e.

There is no contradiction, but we must admit that our choice of word is confusing in the cited paragraph (page 8, lines 25-26). "Monophase patches" intended to describe microstructural domains that contain only one type of pyroxene intermixed with olivine, i.e., small clino- and

orthopyroxene rarely occur intermixed with each other. As the reviewer pointed out, Fig. 3 indeed shows that olivine is often intermixed either with orthopyroxene or with clinopyroxene in these patches, but only rarely with the two mineral phases at the same time in the same domain. This observation is also consistent with the analysis of second phase particles presented in Fig. 8, particularly in the fine-grained xenoliths. We clarified the petrographic description in the revised manuscript: *"…Small orthopyroxene and clinopyroxene are generally present with a proportion ranging from 80:20 to 60:40 in a given xenolith, respectively, and they typically occur in patches rich in small olivines that are heterogeneously intermixed with either clino- or orthopyroxene (Fig. 3e). Phase mixing between the two pyroxenes is rare in such domains…"*

Page 12, Lines 23-25: Development of axial-[100] CPO symmetry in olivine has also been attributed to constrictional strain (Chatzaras et al., 2016).

We included this reference in the revised paragraph.

Page 13, Lines 15-30: I do not think that the one hypothesis necessarily precludes the other. Olivine shearing in the presence of melt could take place in transpressional deformation, where the (001)[100] and (010)[100] (as suggested by the concentration of rotation axes around [001] in Figure 6 for the fine-grained xenoliths) olivine slip systems could both be active due to strain compatibility requirements.

We added this alternative to the text: *"…Alternatively, the transition of olivine CPO symmetry toward axial-[010] in the fine-grained xenoliths may have developed enhanced by several of the above factors, of which the most likely scenario would be focused melt migration in a transpressional mantle shear zone, considering the geodynamic environment of the Oran volcanic field…"*

Page 14, Lines 14-15 and 22: Please name the deformation mechanisms.

We clarified the sentence in the revised version: *"…These observations attest for the increasing impact of melts on the deformation from coarse-grained to fine-grained microstructures…"*